Chitin-binding protein behavior at chitosan interface studied by quartz crystal microbalance with dissipation monitoring (QCM-D): Binding quantification, orientation and affinity constants

Lisa Basso, Clémence Vuillet, Yvan Rahbé, Laurent David, Aurélia Charlot, Guillaume Sudre

Chitin-binding protein behavior at chitosan interface studied by quartz crystal microbalance with dissipation monitoring (QCM-D): binding quantification, orientation and affinity constants

Lisa Basso [a], Clémence Vuillet [a], Yvan Rahbé [b], Laurent David [a], Aurélia Charlot [a], Guillaume Sudre [a]

[a] *Universite Claude Bernard Lyon 1, INSA Lyon, Université Jean Monnet, CNRS UMR 5223, Ingénierie des Matériaux Polymères (IMP) F-69622 Villeurbanne Cédex, France.*

[b] *Universite Claude Bernard Lyon 1, INSA Lyon, INRAE, CNRS UMR 5240, Microbiologie, Adaptation et Pathogénie (MAP), F-69621 Villeurbanne, France*

Keywords: Protein, quartz crystal microbalance (QCM-D), Wheat germ agglutinin (WGA), Chitosan, Chitin-binding domain (CBD)

Published in *Colloids and Surfaces B: Biointerfaces*:

Chitin-binding protein behavior at chitosan interface studied by quartz crystal microbalance with dissipation monitoring (QCM-D): binding quantification, orientation and affinity constants. **Basso L., Vuillet C., Rahbé Y., David L., Charlot A., Sudre G.**, *Colloids and Surfaces B: Biointerfaces*, **2025**, *252*, 114650.

Link to the publisher version: https://doi.org/10.1016/j.colsurfb.2025.114650

Graphical abstract

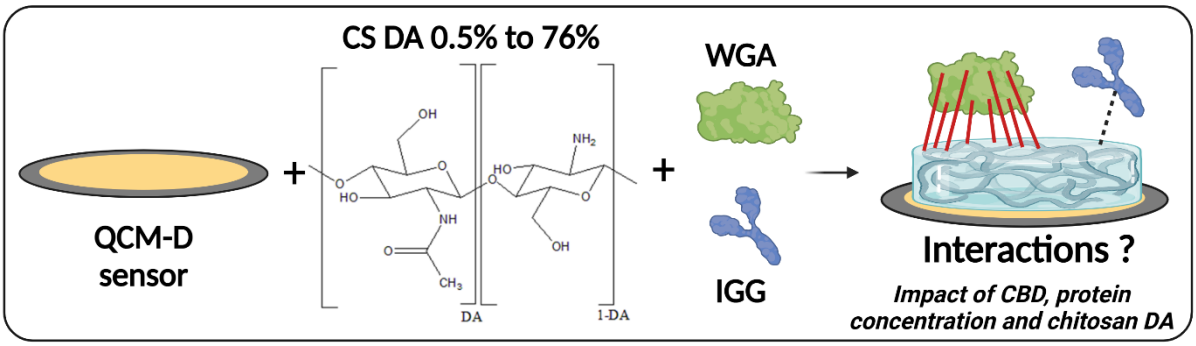

When having a chitin-binding domain, the interaction of proteins with chitosan depends on DA and on protein concentration, with a two-step association mechanism at high concentration.

Abstract

A full comprehension of chitosan interaction with proteins is yet to be achieved, in view of the complexity of the physico-chemical behaviors found in the chitosan family, and the diversity of possible protein interaction mechanisms. In this work, we studied the interactions between chitosans and wheat germ agglutinin (WGA), a lectin that can bind chitin thanks to an amino-acid pattern called the hevein-like chitin-binding domain (CBD). The specificity of CBD interactions with chitin/chitosan chains and the impact of the degree of acetylation (DA) of chitosan have been studied by quartz crystal microbalance with dissipation monitoring (QCM-D). The mass per unit area of WGA adsorbed on chitosan was six times higher than that of immunoglobulin G (IGG), which does not contain a CBD. The mass per unit area of deposited WGA was also almost twice as high at higher chitosan DAs (54%, 67%, 76%) than at lower DAs (0.5%, 15%, 35%), evidencing more specific interaction with “chitin-like” chitosans. WGA is a dimer at neutral pH and presents 4 CBDs on each monomer. The repartition of these CBDs seems to allow for reorganization of WGA on the chitosan surface in order to favor the interactions of this chitosan with a higher number of proteins. Furthermore, the binding kinetics have been assessed and modelled with a two-step association model, providing insights on the observed association constants. These results indicate that QCM-D constitutes a suitable method for the analysis of lectin CBD–chitosan dynamic interactions and could be applied to other types of proteins, in particular CBD proteins or further used in biosensor elaboration or biomaterial coating assessment with chitosan of different DAs.

1. Introduction

Carbohydrate-protein interactions are ubiquitous in various biological processes and are also crucial for many biotechnological applications like therapeutics or biointerfaces [1–6]. Chitin and chitosan are natural copolysaccharides composed of *N*-acetyl-D-glucosamine (GlcNAc) and D-glucosamine (GlcN) residues linked by β (1→4) glycosidic bonds. Chitosan is the product of deacetylation of chitin resulting in a soluble polymer family in acidic aqueous media [7]. Each chitosan can be characterized by the molar fraction of acetylated units (DA), the molar mass distribution, and also the acetylation pattern [8–11]. Chitin can specifically bind proteins which present, along their sequence, a motif of several conserved amino acids called the chitin-binding domain (CBD). In the case of some major plant lectins, this domain is also called the *hevein* domain [12]. This domain allows proteins such as wheat germ agglutinin (WGA) to bind chitin associated with a plant stressor (e.g. insect or fungus) [13]. The hevein domain comprises 30 to 45 amino acids and its interactions with GlcNAc was studied by NMR,[14–20] and X-ray structural analyses [21–23]. It is believed that a few tyrosine and serine residues play a crucial role in this specific binding [21–24]. Lectin carbohydrate interactions have also been studied by isothermal calorimetry in solution [25,26]. The potential for lectin-carbohydrate biosensors recently raised interest and motivated studies involving quartz crystal microbalance with dissipation monitoring (QCM-D) and surface plasmon resonance (SPR) to quantify and characterize the interactions between the lectin and the polysaccharide [1,3,26–31]. QCM-D allows for the determination of surface interactions at very low scale (sensitivity up to 1 ng/cm²) providing insights on affinity rate constants and binding energies and can be used for various applications. Carbohydrate-lectin QCM-D studies can present different experimental setups. The component immobilized on the sensor surface is either the carbohydrate [1,3,29,30] or the lectin [31]. The study of the interactions of WGA with different types of monosaccharide modified QCM-D sensors showed preferential interaction of WGA with GlcNAc compared to other types of monosaccharides like mannose and galactose [3]. Wangchareansak *et al.* studied the Langmuir parameters for the interaction between a WGA solution and GlcNAc coated sensor and defined two distinct binding regimes according to the concentration of WGA used in the system [28]. So far, apart from this last study, only monosaccharides (GlcNAc) were used to study CBD

interactions of WGA by QCM-D. To the best of our knowledge, no QCM-D experiments involving the entire unmodified chitin/chitosan chain interactions with lectin has been reported yet. Moreover, the impact of the degree of acetylation (DA) of chitosan was not assessed. As seen in the literature, it is possible to obtain reacetylated chitosans up to a DA of 80% [32]. These highly reacetylated chitosans could act as chitin-like polymers soluble in acidic water and can be used for coating of QCM-D sensors to study the interactions of proteins with chitosan of low and high DA giving rise to further insights on CBD interaction mechanisms.

This article is the first to present a QCM-D study of the dynamic interactions of a CBD protein, WGA, with unmodified chitosan whole chains of different DAs up to 76%. This article presents the adsorption of WGA compared to IGG on chitosan-coated sensors, the study of WGA interaction with chitosan of different DAs and at different concentrations of protein and provides insights into CBD interaction mechanisms. The binding rates of WGA adsorption were also assessed.

2. Materials and methods

2.1. Materials

A detailed list of raw materials used in this study and corresponding sources can be consulted in the Supplementary Materials, SM.

2.1. Preparation of reacetylated chitosans

Chitosan powder was solubilized in an aqueous acetic acid solution (polymer concentration c_p = 0.5% w/v, $n_{AcOH} = n_{GlcN}$). Insolubles were removed by successive filtration through cellulose membranes of pore sizes of 3 µm, 1.2 µm and 0.45 µm. Chitosan was retrieved from the solution by precipitation allowed by increase in pH to 10 by ammonia solution addition. The precipitate was then washed against distilled water until neutral pH and freeze-dried to obtain a purified chitosan powder. Reacetylation of the purified chitosan was achieved thanks to a process previously described by Vachoud *et al* [33]. Briefly, chitosan was dissolved in an acetic acid aqueous solution and an equivolume of 1,2-propanediol was then added. Acetic anhydride was added stoichiometrically to GlcN units of chitosan intended to

be reacetylated. After stirring for 12 h, the reacetylated chitosans were precipitated, washed and freeze-dried and chitosan powders of DAs 15%, 35%, 54%, 67% and 76% (+/-1%) were obtained. Again, the estimation of the DAs was performed by ^{1}H NMR (Bruker advance III, 300MHz, 64 scans) using the Hirai *et al.* method [34]. Mass average molar masses were determined by size exclusion chromatography (SEC-MALLS). Chitosans were dissolved in AcOH/AcONa (0.2 M/0.15 M) buffer (pH 4.5) to a concentration of 0.5 mg/mL and the refractive index increment was adjusted for every DA according to the method described previously [32,35].

2.2. QCM-D preparation and measurements

2.2.1. Chitosan and protein solutions

Chitosans solutions were prepared by solubilizing chitosan powders in aqueous acetic acid solutions (c_p = 1% w/v, $n_{AcOH} = n_{GlcN}$). The chitosan solutions were then diluted to 0.5 mg/mL in 0.15 M NaCl (at pH 5.5) for QCM-D analysis. Proteins (WGA or IGG) were diluted to either 10 or 50 µg/mL in HEPES buffer (0.01 M, pH 7).

2.2.2. QCM-D measurements

Sensors were cleaned by successive rinses with milli-Q water and ethanol and subjected to ozone treatment (UVO-CLEANER® Model 42 SERIES) for 20 min. The sensors were then placed in the fluidic cell of the Qsense Explorer (Biolin Scientific, Sweden) and flushed with the analyte buffer to establish a stable baseline (*i.e.* NaCl for chitosans and HEPES for proteins on bare gold). The solutions were filtered at 0.8 µm and injected in the system at 100 µL/min. After any change in analyte solution, the system was left to equilibrate until a stable resonance frequency was reached (time to reach equilibrium depends on the analyte solution, for example ~ 30 min for chitosan deposition on QCM-D gold sensors and around ~ 150 min for WGA deposition on chitosan layer). A typical measurement cycle consisted of: (*i*) establishing the baseline with NaCl (0.15 M, pH 5.5); (*ii*) injecting the chitosan solution (0.5 mg/mL in NaCl 0.15 M pH 5.5) into the sensing chamber; (*iii*) washing of the deposited chitosan by injecting the NaCl baseline buffer (0.15 M, pH 5.5) to remove the weakly adsorbed chitosan; (*iv*) equilibration of the sensor with the HEPES solution (0.01 M, pH 7); (*v*) injection of the protein

solution (WGA or IGG at 50 µg/mL or 10 µg/mL in HEPES buffer, pH 7) in the QCM-D cell and run until equilibration and (*vi*) washing of the protein layer with a solution of HEPES buffer (0.01 M, pH 7) to remove poorly immobilized proteins. The washing steps allow to analyze the reversibility of the adsorption. After the experiment, the sensor was unmounted and washed with the previously described water/ethanol and ozone process 3 times, dried with N_2 and stored until further use. The sensors were not used for more than 5 successive experiments. In order to thoroughly wash the QCM-D fluidic cell, a milli-Q water solution was flushed, and the device was unmounted and washed with milli-Q water.

2.2.3. QCM-D data analysis

The Qsoft software was used for data collection. During the experiments, after application of a voltage, the crystal sensor oscillates to its resonance frequency and the 3rd, 5th, 7th, 9th and 11th overtone of this frequency were recorded, as well as the energy dissipation shift of the signal (only the 5th overtone results will be presented here). The Qsense Dfind software was used for data analysis. Considering that the deposited polymer forms a rather thin and rigid film [relatively low $\Delta D_n/n$ ($< 5 \times 10^{-6}$) for any of our experiments, and good superimposition of all overtones], the Sauerbrey equation (equation 1) was used to model the collected data and convert the resonance frequency shift of the 5th overtone to the adsorbed mass of analyte per unit area:

$$\Delta m = \frac{-C\Delta f}{n} \quad (1)$$

Where C is the mass sensitivity constant (17.7 ng/cm^2/Hz at 5 MHz), n the overtone number and Δf the change in resonance frequency of the n^{th} overtone.

Exponential and bi-exponential functions were used to fit the experimental data and determine affinity constants. Details on data analysis and fitting functions can be consulted in SM.

3. Results and discussion

3.1. Characterization of chitosans

The commercial chitosan powder was purified and reacetylated to DAs of 0.5%, 15%, 35%, 54%, 67% and 76% as assessed by ^{1}H NMR (spectra can be consulted in Basso *et al.* [36]). The molar masses were in the range M_w= 200-300 kg.mol^{-1}, results can also be consulted in Basso *et al.* [36].

3.2. CBD proteins present specific interactions with chitosans

The interactions between "chitin-like" chitosan of DA 76% or chitosan of DA 0.5%, with either WGA or IGG were studied by QCM-D and compared. IGG presents an isoelectric point of 8.0 [37], not far from the isoelectric point of WGA of 8.7 [38]. The studies were first conducted at pH 7, at which both proteins are slightly positively charged. The results are presented in Figure 1(a).

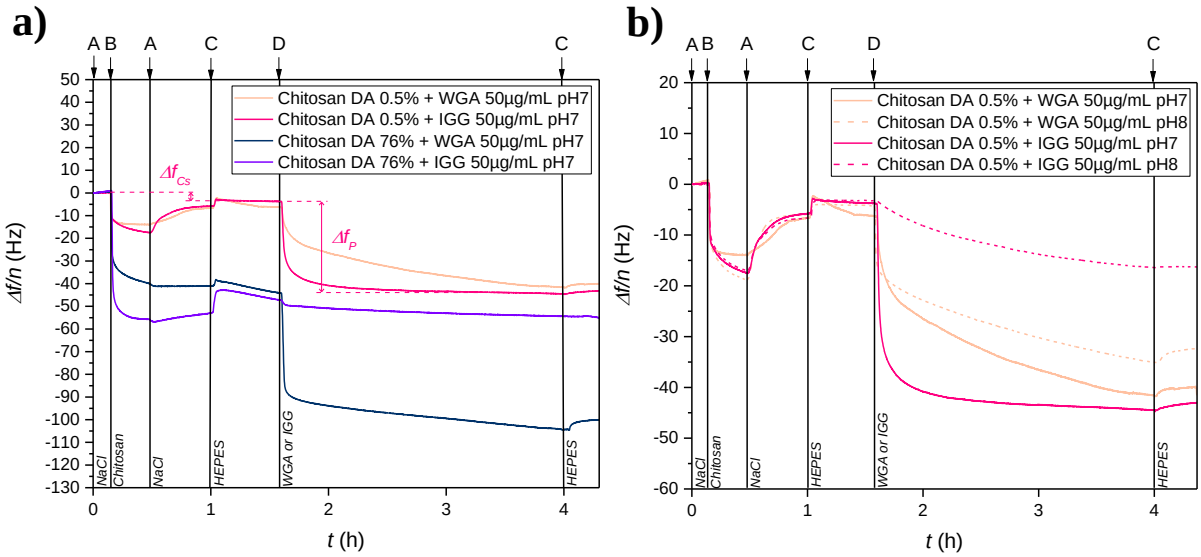

Figure 1: (a), QCM real-time adsorption monitoring of chitosan of DA 76% or chitosan of DA 0.5% and proteins (WGA, orange and blue, respectively; IGG pink and purple, respectively) at pH 7. (b), QCM real-time adsorption monitoring of chitosan of DA0.5% and proteins (WGA, orange and IGG pink) at pH 7 (solid line) and pH 8 (dashed line). The letters A, B, C and D indicate the different solutions injected in the QCM-D chamber (A: [NaCl] = 0.15 M pH 5.5; B: Chitosan of DA 0.5% or DA 76% at 0.5 mg/mL in buffer A; C: HEPES at 0.01 M and pH 7 or pH 8; D: Protein (WGA or IGG) at 50µg/mL in buffer C). The frequency changes are labelled by a double arrow for the adsorption of chitosan (Δf_{CS}) and the adsorption of the protein (Δf_P). The changes in solution flows are marked with their corresponding letters.

A layer of chitosan was deposited (B) onto the gold sensor and a solution of 50 µg/mL of proteins was then injected (D) in the QCM-D system. Before protein adsorption and after rinsing with NaCl solution and HEPES buffer (t = 90 min), the frequency shifts resulting from chitosan adsorption for DA 0.5% and DA 76% slightly differ from one experiment to the other but stabilize at Δf_{Cs} = −4 Hz for DA 0.5% and −40 Hz for DA 76%, the differences in chitosan adsorption will be discussed below. For chitosan of DA 76% at pH 7 (Figure 1 (a)), the frequency shifts resulting from protein deposition were equal to Δf_P = −56 Hz for WGA and −7 Hz for IGG after a time of around 2.5 h for both proteins with a fast adsorption in the first few minutes (adsorption kinetic will be discussed and quantified hereafter). This shift in frequency corresponds to a mass per unit area of protein of 999 ng/cm^2 and 165 ng/cm^2 for WGA and IGG, respectively, as deduced from equation (1). There is more than a 6-fold difference between the two results. IGG presents a molar mass 4 times higher than WGA (150 and 36 kDa, respectively) which means that at same adsorbed mass, 4 times more molecules of WGA are adsorbed than IGG. The mass adsorbed during the experiment is 6 times higher for WGA than for IGG, so, ultimately 24 times more molecules of WGA are immobilized than IGG. For chitosan of DA 0.5%, the frequency shifts resulting from protein adsorption were around −34 Hz for WGA and −39 Hz for IGG, corresponding to surface densities of 602 and 698 ng/cm^2, respectively. Thus, no clear difference in the adsorbed mass of the two proteins can be distinguished in the low DA case, possibly because (*i*) at DA 0.5%, less chitosan is immobilized on the gold sensor; and (*ii*) WGA interaction with chitosan is thus less distinguishable than at DA 76% where the CBD may play a more impacting role. As a comparison, for a control experiment on bare gold without the presence of chitosan, this value is reduced to 400 ng/cm^2 for WGA absorption and increased to 930 ng/cm^2 for IGG (possibly adsorbed via amine chelation with gold or electrostatic interactions as WGA and IGG are slightly positively charged at pH 7, see Fig. S1).We can deduce that the presence of chitosan limited the adsorption of IGG onto the gold surface of the sensor and favorized that of WGA, evidencing unspecific interactions controlling the adsorption of IGG and the specific interactions formed by WGA with chitosan. In order to evidence the contribution of electrostatic interactions in protein immobilization, the interactions between chitosan of DA 0.5% and WGA or IGG were conducted at pH 8 (Figure 1 (b)). At pH 8 (dashed lines), the frequency shifts for

the adsorption on chitosan of DA 0.5% are reduced to −28 Hz for WGA and −12 Hz for IGG (corresponding adsorbed masses of 500 and 234 ng/cm^2, respectively). The significant reduction in IGG binding when increasing pH suggests that binding to chitosan is favored by electrostatic interactions. The binding of WGA is rather weakly affected by the change in pH, confirming the specific affinity of WGA to chitin and chitosan through its CBDs. WGA appears to present specific interactions with both chitosans of DA 0.5% and 76%: this result means that the CBD can be experimentally confirmed as a chitosan-binding domain and not solely a chitin-binding domain. However, the amount of bound WGA is higher at DA 76% than at DA 0.5% (Figure 1 (a): 999 ng/cm^2 and 165 ng/cm^2 for WGA and IGG, respectively) suggesting that the interaction of WGA with "chitin-like" chitosan is favored, which is characteristic of the CBDs of WGA. These results are also quantitatively within the frame of previous literature on the subject. The quantification, by fluorescence microscopy, of WGA on chitosan-coated surfaces of same DA of 76% presented a mass per unit area of protein of 477 ng/cm^2 [36]. Sugawara *et al*. studied the adsorption of WGA on chitin films by voltametric analyses and reported a mass per unit area of 774 ng/cm^2 [39]. The observed differences can be due to different configurations of WGA binding on the surface (ex: "in-plane" and "out-of-plane" bindings) allowing deposition of more or less WGA (this hypothesis will be detailed below).

3.3. Chitosan DA impacts the amount of interaction sites with CBD proteins

The adsorption of WGA onto chitosan was studied for a homologous series of chitosans with similar molar masses but with different DAs (0.5%, 15%, 35%, 54%, 67% and 76%) using a constant concentration of protein of 50 µg/mL (Figure 2).

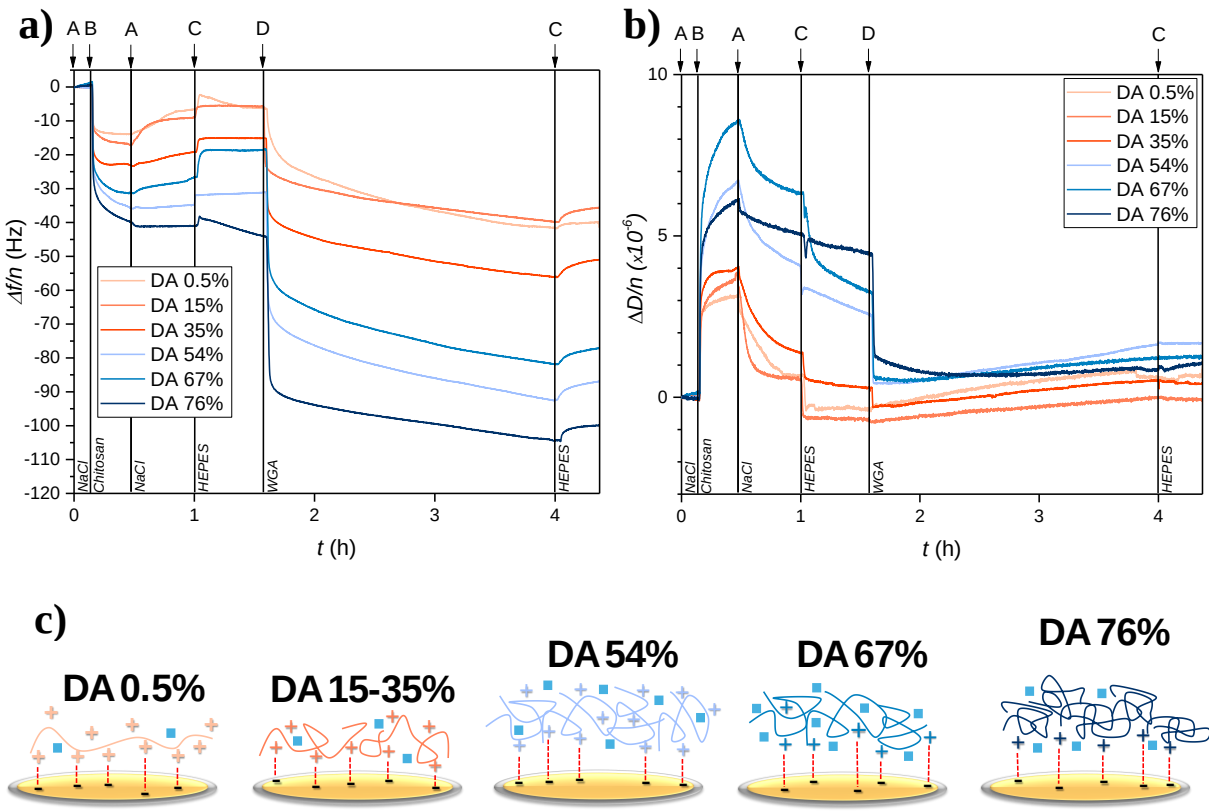

Figure 2: QCM-D real-time adsorption monitoring of chitosan of different DAs (0.5%, 15%, 35%, 54%, 67%, and 76%) and WGA: (a) frequency shift and (b) dissipation shift. The letters A, B, C and D indicate the different solutions used in the system (A: [NaCl] = 0.15 M at pH 5.5; B: Chitosan at 0.5mg/mL in buffer A; C: HEPES at 0.01 M and pH 7; D: WGA at 50 µg/mL in buffer C). The changes in solutions are marked by an arrow with the associated letter and a vertical bar. For more clarity, a graphical representation of the conformation adopted by chitosan chains during the adsorption at pH 5.5 on gold sensors is presented in (c). Blue squares represent water molecules responsible for chitosan swelling and higher dissipation.

Firstly, we can observe that the frequency shifts after washing of the deposited chitosan layer were of −6 Hz for DAs 0.5% and 15%, around −14 Hz for DA 35%, −31 Hz for DA 54%, −18 Hz for DA 67% and −44 Hz for DA 76%. These results indicate that the amount of deposited chitosan onto gold sensors gradually increases with the DA apart from the deposition of chitosan of DA 54% which leads to an enhanced adsorption compared to chitosan of DA 67%. The adsorbed mass per unit area and thicknesses, at the swollen state in aqueous medium calculated from the resonance frequency changes are presented in Table 1.

Table 1: Mass per unit area and thicknesses of chitosan layers and WGA layers on the QCM-D sensor calculated from the frequency shifts and Sauerbrey equation (error on mass was estimated inferior to 1 ng/cm² by Dfind Sauerbrey analysis). The thicknesses were deduced from the deposited mass (error on thickness was estimated inferior to 0.01 nm). A density of 1050 g/L (hydrated sugar, Dfind software) was chosen for chitosan and a density of 1100 g/L was chosen for WGA (hydrated protein density, Dfind software).

DA (%)	Mass per unit area of chitosan (ng/cm^2)	Thickness of chitosan layer (nm)	Mass per unit area of WGA (ng/cm^2)	Thickness of WGA layer (nm)
0.5	113	1.0	602	5.5
15	103	1.0	532	4.8
35	271	2.6	633	5.6
54	558	5.3	986	8.7
67	332	3.2	1043	9.3
76	787	7.5	999	8.7

Low DA chitosans carry $–NH_2$ groups which are partially positively charged at pH 5.5. The chitosan chains can thus interact with the negatively charged gold sensor by electrostatic interactions (presence of an OH- adlayer on QCM-D sensors in aqueous environment, sensor charge was verified with zeta potential in NaCl at pH 5.5) [40]. High DA chitosan present less (potentially ionized) $–NH_2$ groups. More chitosan chains are then needed to counter the negative charges at the surface of the gold sensor and consequently a higher mass of chitosan could be deposited at high DA. Moreover, the extend of repulsive electrostatic forces between chitosan chains (dependent of the DA), is anticipated to play on the conformation adopted by the adsorbed chitosan chains and thus the obtained mass per unit area. At low DA, such repulsions are at the origin of the observed lower mass of deposited chitosan, explained by the expansion of the adsorbed polymer chains at the surface (see Figure 2 (c)). In parallel, the dissipation was monitored during chitosan deposition (Figure 2 (b)). Two ranges of dissipation energy variations are observed: the first one with relatively low dissipation at low DA (0.5% to 35%) and a second one with a pronounced dissipation for higher DA (54% to 76%), as a consequence of the differences in the deposited mass of chitosan, gathered in Table 1.

Such changes in dissipation as a function of the DA corroborates the fact that the DA (at a given pH) closely controls the conformation of the chitosan chains in aqueous solution and at the surface of the gold sensor. Given that at high DA, electrostatic repulsive forces are screened, polysaccharide chains are less extended and are adsorbed onto the surface under the form of globules and coils that are able to entrap a higher number of water molecules. This peculiar chain conformation leads to an increase of both: *(i)* the mass of deposited chitosan and *(ii)* the amount of water molecules embedded within the polymer chains. Herein, the DA increase yields an enhancement of the hydration and swelling degree of polymer chains. Moreover, the tricky differences in dissipation shifts observed between the three high DA values (54%, 67%, and 76%) can be attributed to the distribution/repartition of the D-glucosamine and *N*-acetyl-D-glucosamine units along the chitosan backbone, which might impact the conformation in solution and thus the degree of compacity of the layer. The distribution of these repetitive units can also play on the extent and the strength of the interactions (electrostatic interactions involving $-NH_3^+$ groups and chelation involving $-NH_2$ groups) developed at the interface with the gold sensor.

The amount of bound WGA increases with DA and a gap is observed once again between the two ranges of DA: low DAs (0.5%, 15%, 35%) and high DAs (54%, 67%, 76%). This trend was previously evidenced for WGA interaction with chitosan-grafted films of different DAs quantified by fluorescence microscopy and was attributed to the increased affinity of WGA's CBD for "chitin like" chitosans of high DA [36]. By considering thicknesses and the swelling degrees of chitosan layers, we can speculate that WGA proteins are able to interact with the surface of the chitosan layer and diffuse in the depth of the layer to interact with additional available interacting sites. As a result, the differences in WGA interaction with chitosan of different DAs is subtle and can thus be modulated by *i)* the specific interaction of WGA with chitin-like chain portions, *ii)* the thickness of the chitosan layer and *iii)* the ability of chitosan to swell in aqueous media [41,42]. Nevertheless, for quasi-identical thicknesses of chitosan layer for DAs 35% and 67%, a pronounced difference in the amount of WGA bound to the chitosan layer is observed (633 for DA 35% against 1043 ng/cm^2 for DA 67%). Consequently, we can conclude that the high mass per unit area of WGA adsorbed chitosans of high DAs is linked to the higher affinity of WGA CBD for chitin-like chitosans (bearing more GlcNAc units). Additionally, the

adsorption of the protein quickly occurred, and the interaction seem very strong as no desorption is observed during the washing step.

3.4. Proteins are subjected to changes in binding configuration to present more interaction sites with chitosan

3.4.1. Impact of protein concentration

Monitoring of protein adsorption on chitosan of DA 0.5% was performed at two WGA concentrations, *i.e*. at 50 µg/mL (high concentration, noted HC) or 10 µg/mL (low concentration, noted LC). It may be noticed that the frequency shift resulting from WGA deposition on the chitosan layer is almost twice as high for WGA at HC than for WGA at LC (−41 Hz and −24 Hz, respectively, see figure S2): although we have let adsorption to occur until equilibrium, the surface densities of WGA are estimated at 602 ng/cm^2 at HC and 295 ng/cm^2 at LC. These results show that the concentration of the solution strongly impacts the amount of adsorbed WGA. To go a step further in the elucidation of such adsorption regimes, we can study both adsorption-induced changes in frequency (mass adsorbed) and dissipation (viscoelasticity/hydration rate of the layer): the plots of the variation in dissipation ($\Delta D/n$) as a function of the variation of frequency ($\Delta f/n$), also called the "ΔD-Δf plots", can be used to gain information on the binding characteristics of the interaction (Figure 3), from the examination of the dissipation changes per unit of adsorbed mass.

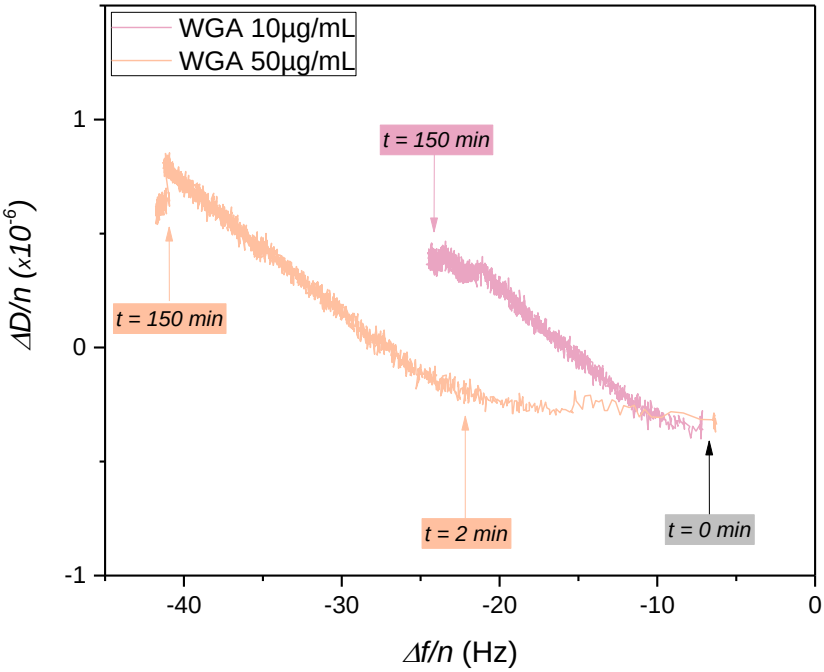

Figure 3: ΔD-Δf plots of the adsorption of WGA solutions at two different concentrations (50 and 10 µg/mL) on chitosan of DA 0.5%. For WGA at HC, protein adsorption presents 2 domains: the first one is a decrease in frequency at constant dissipation (horizontal slope) and the second one is a decrease in frequency with increased dissipation. For WGA at LC, protein adsorption presents a sole domain: a decrease in frequency with increase of dissipation.

For WGA at HC, two domains can be evidenced. For the first 2 min, the frequency rapidly decreases from −6 Hz to around −23 Hz without significant dissipation change (horizontal slope, Figure 3). After that, for the rest of WGA binding (around 2 h), the frequency decreases from −25 Hz to −45 Hz with an increase in dissipation presenting a negative slope in the Δ*D*-Δ*f* plot. This slope is identical to the slope observed for binding of WGA at LC, which does not present the first horizontal domain. Such a slope change for protein adsorption has previously been observed and attributed to a distinct conformational change of the protein on the surface [43–47]. Hampitak *et al.* described a two-step adsorption mechanism for BSA on graphene, characteristic of hydrophobic interactions followed by hydrophilic interactions: BSA hydrophobic sites are adsorbed first in an "in-plane" configuration followed by the hydrophilic ones located at the extremity of the protein and resulting in an "out-of-plane" protein configuration [46]. Komorek *et al.* studied the deposition of lysozyme by QCM-D and a two slope response of the Δ*D*-Δ*f* plot was associated to a reorganization of the lysozyme layer [47]. As each WGA monomer presents 4 CBDs (adding up to 8 for the dimer), it has been previously discussed that WGA can adsorb on chitosan with different binding configurations [28]. The protein can then interact "out of

plane" with CBDs located at the extremity of the protein with the chitosan surface or the interaction could involve more CBDs stabilizing the protein in a configuration "in-plane" where the protein takes up more space on the surface (see Fig. S3 for details on "in-plane" and "out-of-plane" WGA configurations) [28].

Considering this information, we can hypothesize that in our experiments, for WGA at LC, the protein interacts "in plane" in regards to the chitosan layer whereas at HC the protein first interacts "in plane" as a low dissipation compact layer of proteins, but then, the protein layer is subjected to a progressive reorganization to an "out-of-plane" configuration that allows to increase the number of interaction sites and thus enhance further binding of WGA onto the chitosan layer. It has to be noted that WGA "in-plane" binding is expected to present identical and even super-imposable slopes on the ΔD-Δf plot for HC and LC if the surface presents the same organization [48]. The differences in slopes observed may be explained by the differences in concentration. At high concentration, the surface gets rapidly saturated with "in-plane" WGA due to a high influx of protein, without allowing chitosan chain rearrangement. This results in a more horizontal (flat) curve, indicating a quick adsorption phase (2 minutes) of "in-plane" proteins. At low concentration, WGA adsorbs gradually, leading to a continuous slope with increase in dissipation as the adsorption progresses over time and the layer appears more viscoelastic as proteins are less tightly packed.

As presented above, the characteristic two-slope response in the ΔD-Δf plot of WGA binding is characteristic of layer reorganization; additionally, the deposited protein amounts as well as the corresponding thicknesses of the protein layer are consistent with this model (Table 2).

Table 2: Masses and thicknesses of chitosan layer and WGA layer on the QCM-D sensor calculated from the frequency shifts and Sauerbrey equation when conducting experiments with high and low concentration of WGA (10 and 50 µg/mL). The error on mass was estimated inferior to 1 ng/cm^2 and the error in thickness inferior to 0.01 nm. The thicknesses were deducted from the deposited mass and a density of 1050 g/L (hydrated sugar as presented in the Dfind software) was chosen for chitosan. A density of 1100 g/L was chosen for WGA (hydrated protein as presented in the Dfind software).

	WGA at 10 µg/mL (LC)	**WGA at 50 µg/mL (HC)**
Thickness of chitosan (nm)	1.2	1.1
Mass of WGA before slope change in the ΔD-Δf plot (ng/cm^2) ($\Delta f = -22$ Hz)	-	291
Final mass per unit area of WGA (ng/cm^2) ($\Delta f = -40$ Hz for WGA at HC and $\Delta f = -22$ Hz for WGA at LC)	295	602
Final thickness of WGA (nm)	2.6	5.4

For WGA at HC, the mass per unit area of bound proteins is equal to 291 ng/cm^2 before the slope change on the ΔD-Δf plot, which is similar to the mass per unit area resulting from the binding of WGA at LC. This would mean that the protein first deposits "in plane" for both systems (HC and LC) leading to the same amount of deposited protein for both concentrations. After that, for HC, the proteins are subjected to a change in interaction to an "out-of-plane" configuration allowing for the deposition of a higher quantity of WGA (from 295 ng/cm^2 to 602 ng/cm^2). The results also match with the theoretical amounts of WGA leading to saturation of the sensor surface. If we consider the WGA dimer as an ellipsoid resulting from the head to tail interaction of the horseshoe shaped monomers of WGA (see fig. S3 and Uniprot®: P10968 for 3D representations of WGA dimer), then the surface taken by a single WGA dimer interacting "in plane" is an ellipse of 3.8 nm minor diameter and 6.7 nm major diameter (as measured on 3D structure of PDB: 2UVO, see Fig.S3); one single protein takes 20 nm^2 on the surface. This corresponds to a mass per unit area of protein of 298 ng/cm^2 for full sensor surface. This result is in accordance with the amount of proteins bound to the surface for experiments with WGA at LC (295 ng/cm^2). If WGA interacts "out of plane" with the chitosan surface, the area taken by the protein can be simplified to a circle of 3.8 nm in diameter (area of 11 nm^2). The mass per unit area of protein would

thus appear as 536 ng/cm^2. This result is in accordance with the amount of protein bound to the surface for experiments with WGA at HC in the second step of the deposition (602 ng/cm^2). Moreover, the thickness of WGA bound to chitosan at LC is 2.6 nm, which is close to the size of a single layer of "in-plane" WGA (3.8 nm) but still smaller, this could indicate that the protein is denatured or hydrated at the surface or that the dimer is split into two monomers (which is known to be unlikely in solution at pH 7 and room temperature) [49]. For WGA at HC, the final thickness of WGA is 5.4 nm, which is intermediate between the sizes of "in-plane" and "out-of-plane" WGA. The hydrodynamic radius of WGA is close to 5.6 nm, [49] so this confirms that only a single layer of protein is bound to the chitosan surface. This differences in thickness could be explained (*i*) by a configuration for which the proteins would interact vertically but being partially tilted (see fig.S3) [46] or (*ii*) by an intermediate mean thickness of "in-plane" and "out-of-plane" configurations. The thicknesses gathered in Table 2 are calculated from both the density of the layer and the mass of adsorbed proteins, so it might not represent the actual/real geometric thickness of protein adsorbed. Finally, the possibility for monomeric WGA interactions with chitosan can not be completely ruled out, because of the possible presence of a small fraction of monomeric WGA at pH 7.0. In this view, the adsorption phases observed could then be interpreted as the adsorption monomeric WGA in the first phase (horizontal slope), followed by dimerization of WGA in the second phase. This hypothesis is unlikely as WGA is expected dimeric at this pH and temperature. Moreover, the amount of WGA bound to the surface in the second phase is fairly high (300 ng/cm^2), whereas dimerization of a fraction of bound WGA monomers would not be reach this adsorption values alone. Nevertheless, it cannot be excluded that both processes of "in-plane"-"out-of-plane" reorganization and dimerization occur during WGA binding.

3.4.2. Impact of DA

The different binding regimes of WGA on chitosan surfaces were investigated as a function of DA. QCM-D experiments were conducted with chitosans of DA 0.5%, 15%, 35%, 54%, 67% and 76% and

with WGA concentration of 50 µg/mL (HC). The results of the Δ*D*-Δ*f* plot during WGA binding are presented in Figure 4.

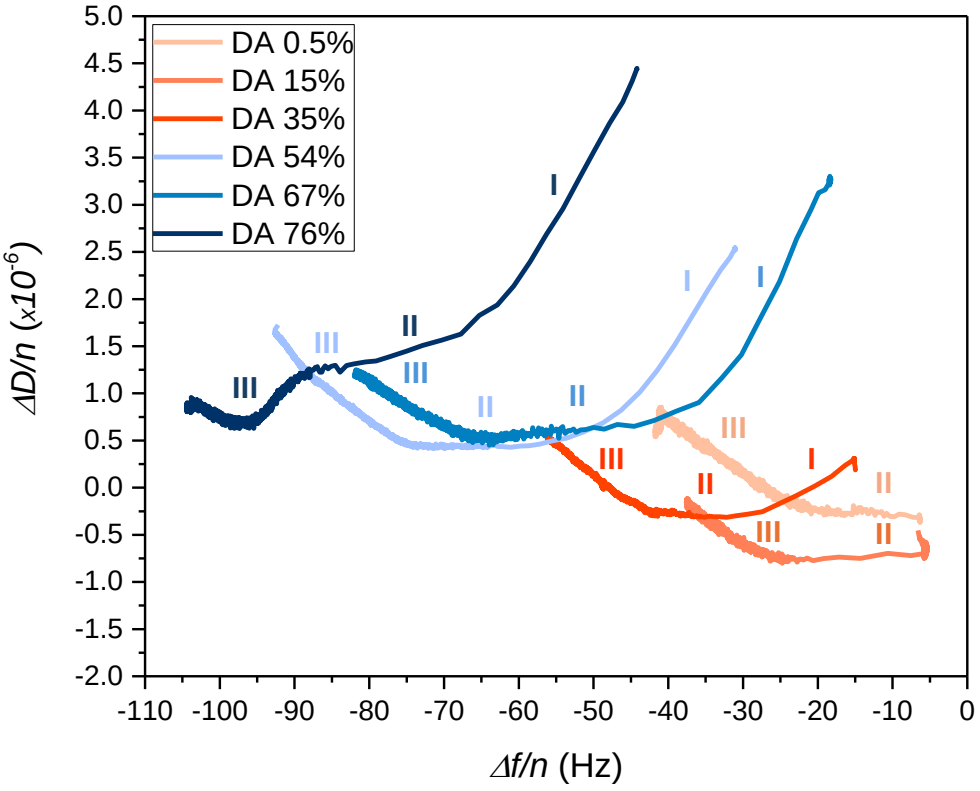

Figure 4: ΔD-Δf plots of the adsorption of WGA (50 µg/mL) on chitosan of different DAs (0.5%, 15%, 35%, 54%, 67%, 76%). The I, II and III symbols represent the different binding regimes observed.

For QCM-D experiments with DAs 0.5% and 15% the behavior is identical. We can differentiate two domains; the first one is the decrease in frequency at constant dissipation (regime II) and the second one is the decrease in frequency with increase in dissipation (regime III), as displayed in figure 4. For DA 15% and above, three separate binding regimes can be distinguished. The first phase consists in a decrease in frequency with a decrease of dissipation (regime I), the second is a decrease in frequency at constant dissipation (II) and the last one a decrease in frequency with an increase in dissipation (III). The first dissipation decrease observed at high DA corresponds to a progressive stiffening of the layer along the deposition of protein [50]. This could be explained by the diffusion and binding of WGA inside the chitosan layer happening at the same time as "in-plane" association and acting as a physical crosslinker causing an increase in stiffness (and a possible deswelling of the chitosan layer). As can be seen in figure 5, the amplitude of the first regime (I), in the Δ*D*-Δ*f* plot, increases with DA. This can be

explained by the increased mass of deposited chitosan at higher DAs thus creating a chitosan layer of higher dissipation (higher ΔD) and higher porosity. The second phase hypothetically corresponds to "in-plane" only interaction of WGA (decrease in Δf with no change in ΔD) and the third phase to "out-of-plane" reorientation of WGA (decrease in Δf with increase of ΔD, "out-of-plane" protein layer appearing more dissipative). The first two deposition regimes happen within 2 to 6 min while the third one lasts approximately 140 min. The slope values of regime (III) do not depend on DA. It can be extrapolated that the proteins adopt the same "out-of-plane" configuration for all DAs. The thickness of deposited protein layer was around 5 nm for DAs 0.5%, 15% and 35%, while the thickness of deposited protein layer was of 9 nm for DAs 54%, 67% and 76% (Table 1). The thickness of the protein layer determined for high DAs seems fairly high and could suggest that WGA does not solely form a single layer on top of the chitosan film (since WGA dimensions do not exceed 7 nm). The calculations in the *Dfind* software only accounts for a translation of the mass deposited to a thickness of layer on top of the precedent layer without including the possibility of protein interaction within the precedent layer. Thus, the results obtained for the protein layer thicknesses are not fully representative of the thickness of WGA layer on top of the chitosan layer, as some of it can be present within the chitosan layer.

3.4.3. Affinity constants

The binding rates are fundamental properties of ligand-receptor systems. In most cases, ligand binding is governed by simple bimolecular interactions. The association step consists in a single ligand binding to a single target site in one step. This binding process is called a one-step association, and the adsorption kinetics (mass adsorbed with time) can be modeled by an exponential function. The observed rate constant k_{obs} takes into account both association and dissociation steps. When the ligand-receptor couple is subjected to changes in conformation, the reaction is considered as a two-step association, and the kinetic data can be analyzed by a bi-exponential function and will imply two separate k_{obs} constants. In agreement with our findings, the interaction of WGA with chitosan can be fitted with an exponential function for low WGA concentration (thus a one-step association corresponding to "in-plane" interaction) and a bi-exponential function for high WGA concentration (meaning a two-step association corresponding to "in-plane" adsorption followed by reorganization to "out-of-plane" configuration). The

modeled curves with bi-exponential functions for high WGA concentration are shown in Figure S4. The association constant tendencies resulting from the data modelling are gathered in Figure 5.

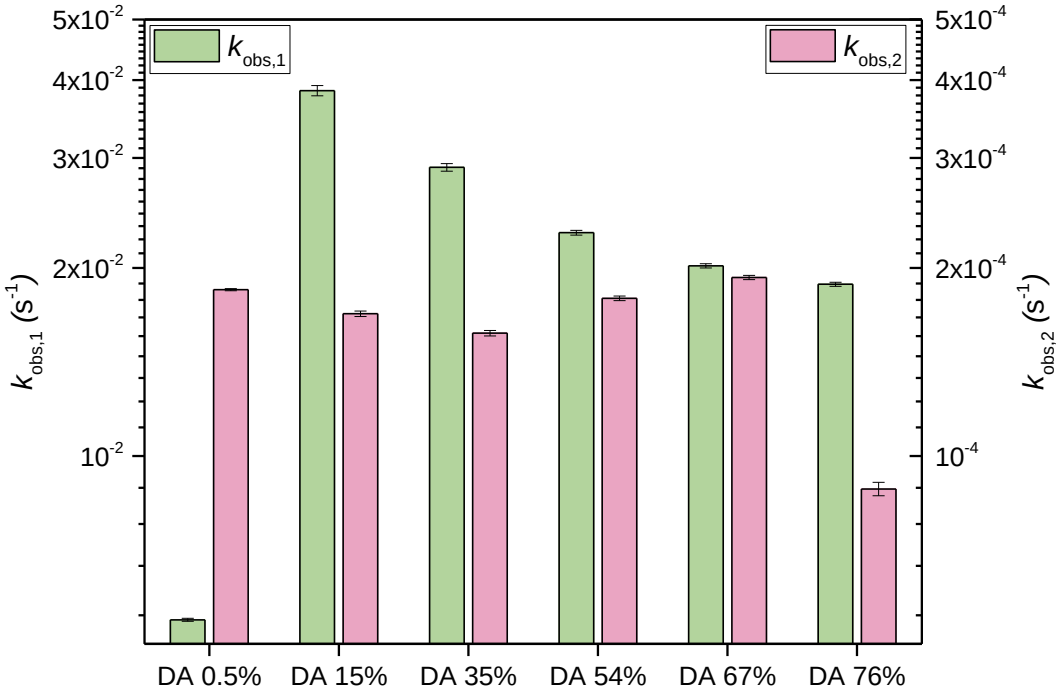

Figure 5: Association rate constants $k_{obs,1}$ (left axis) and $k_{obs,2}$ (right axis) of the adsorption of WGA of concentration 50 µg/mL on chitosan of different DAs (0.5%, 15%, 35%, 54%, 67% and 76%) determined from bi-exponential fitting of the frequency variation during protein binding. Note that the vertical axes are two orders of magnitude apart. Error bars on k_{obs} represent error of bi-exponential fitting.

According to the bi-exponential fitting, the first association phase related to the rate constant $k_{obs,1}$ corresponds both to the primary interaction of WGA with the chitosan layer and to the stiffening of the chitosan sub-layer caused by WGA diffusion within the layer. The two events rapidly and simultaneously occur and present a single association rate constant. The second association phase of rate constant $k_{obs,2}$ relates to the protein layer reorganization. The observed association rate constant $k_{obs,1}$ increases with DA more than ten times between DAs 0.5% and 15%, and then decreases with DA. The increase between DA 0.5% and DA 15%, is possibly due to the presence of GlcNAc groups at DA 15%, which favors specific binding of WGA through its CBDs. The slow decrease at higher DAs can be explained by the diffusion of WGA within the chitosan layer, which could slow the interaction process. The chitosan layer thickness increases with DA, the impact of protein diffusion on association rate constant could appear more important for increased chitosan layer thickness as more WGA is diffused

within the layer. The values of $k_{obs,1}$ at DA higher than 0.5% are consistent with the values obtained by Vogt *et al*. for binding of the CBD of a chitinase (*Bacillus circulans* chitinase A1) with chitin which range from 2.0×10^{-2} s^{-1} to 4.0×10^{-2} s^{-1} [27].

The observed association rate constants $k_{obs,2}$ seem quite constant from DA 0.5% to 35% and increases from DA 35% to DA 67% but then significantly drops for DA 76%. Note that the same amount of bound WGA is obtained for DAs 54%, 67% and 76% (around 1000 ng/cm^2). The decrease observed at DA 76% could be explained by a higher affinity of the CBDs of WGA (upon "in-plane" conformation) for the chitosan of DA 76%, which could hinder and limit layer reorganization. If we hypothesize that the protein interacts in an "in-plane" orientation with chitosan through interaction of more than one of its CBDs, the layer reorganization to "out-of-plane" configuration would require to break one of these bonds to flip the protein to a vertical position where less CBDs are bound to chitosan (see Fig. 6). If the affinity of these bonds is stronger at DA 76%, the energy barrier required to break these bonds would then be higher.

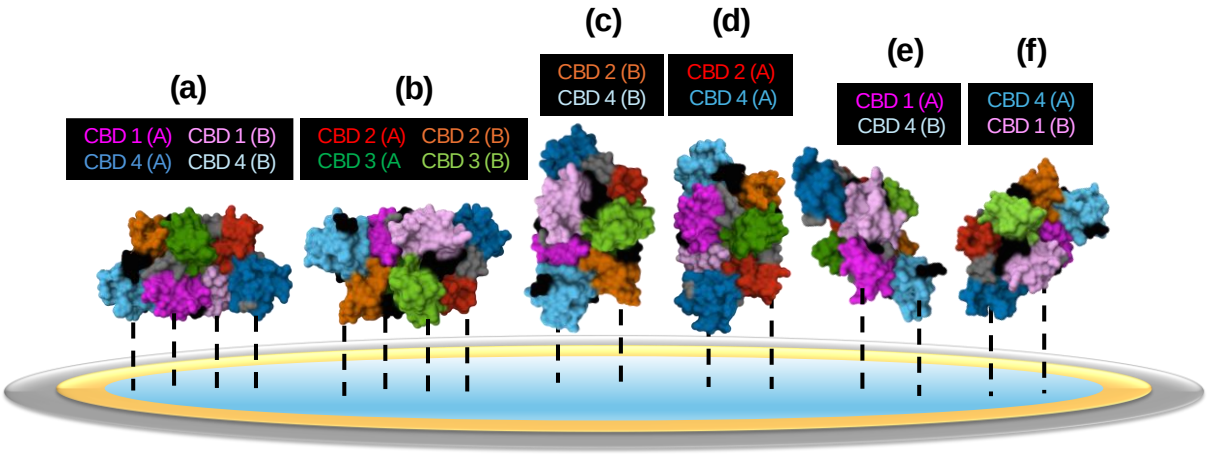

Figure 6: WGA dimer interaction with chitosan on QCM-D sensor. Four CBDs (CBD 1, dark and light pink; CBD2, dark and light green; CBD3, red and orange; and CBD4, dark and light blue) are present on each WGA monomer (monomers noted A, and B). In the first two cases (a) and (b), 4 CBDs from monomers A and B interact with the surface, in the second two cases (c) and (d), 2 CBDs from the same monomer interact with the surface, while in the third two cases (e) and (f), 2 CBDs from different monomers interact with the surface. The dimer protein can appear in plane when it interacts with 4 CBDs or out of plane when it interacts with less than 4 CBDs.

Overall, the rate constant $k_{obs,1}$ is 100 times higher than the rate constant $k_{obs,2}$ for almost all DAs (apart from DA 0.5%). Protein layer reorganization is a slower process compared to the fast primary CBD

interaction of WGA with chitosan. The reorientation process is probably dynamically based on an on-and-off break of some of the CBD bonds and implying the binding of a new protein in the available spot to stabilize the protein in an interaction involving less CBDs. The co-occurrence of these conditions could explain that the "out-of-plane" rearrangement is kinetically slower.

4. Conclusion

We studied, by QCM-D, the CBD interactions of WGA with whole chain chitosans at various DA. The specificity of CBD binding was assessed and compared to other protein interactions and the strong impact of chitosan DA and protein concentration were evidenced. The dynamic affinity constants were also determined for each DA. We were able to demonstrate the specificity of CBD binding of WGA by comparison with the behavior of IGG at pH 7.0 and 8.0. A higher mass per unit area was deposited for WGA compared to IGG and the amount was not impacted by changes in pH compared to IGG. A higher amount of WGA was absorbed on chitosan surfaces of high DAs in comparison with low DAs (almost twice as high) and the maximum mass per unit area was around 1000 ng/cm^2 for DA 67%. As the binding of WGA to chitosan of DA 0.5% was not affected by pH, WGA's CBD can maybe then be considered a "chitosans" binding domain, but with preferred affinity to "chitin-like" chitosans. The concentration of WGA used in the experiment seems to impact the system and cause rearrangement within the protein layer. At a concentration of 10 µg/mL, the proteins probably interact "in plane" with the chitosan layer until saturation of the sensor, while at a concentration of 50 µg/mL, the proteins seem to interact "in plane" until saturation of the sensor and then reorient "out of plane", thus favorably impacting further binding of WGA. Nevertheless, the hypothesis regarding WGA reorientation is still left to be thoroughly examined and would need more in-depth work to be able to be undoubtedly proven. For higher DAs, the protein diffuses within the chitosan sub-layer and interact within the film to access supplementary interaction sites. WGA interaction with chitosan of high DA is a complex multi-step process with a mass adsorption presenting as a two-step process decomposed in three binding regimes with different viscoelastic properties. The observed association rate constants k_{obs} are around 0.02-0.03 s^{-1} for the first association step (interaction of the protein inside the chitosan layer and primary WGA interaction) and 1-2 × 10^{-4} s^{-1} for the second association step (protein layer reorganization). This work shows promising

results in the study of protein interactions with chitosans without the need of a grafted adlayer to help in chitosan immobilization and allows QCM-D experiments with whole chains chitosans of different DAs (0.5% to 76%) and not only GlcNAc monosaccharides. QCM-D constitutes a suitable method for the quantitative analysis of lectin CBD–chitosan interactions and could be applied to other types of CBD proteins such as cuticular proteins which have been less studied. Moreover, the use of chitosan of different DAs in QCM-D opens tremendous perspectives for the development of biosensors or biomaterial coating for which there is a need to tune chitosan DA to assess the affinity of specific proteins.

5. ASSOCIATED CONTENT

Supporting information.

The following files are available free of charge:

- **Figure S1:** QCM-D frequency shifts results for adsorption of WGA and IGG on bare gold sensors.
- **Figure S2**: QCM-D frequency shifts results for adsorption of WGA of concentration 50µg/mL or 10µg/mL on chitosan DA0.5%.
- **Figure S3**: WGA dimer protein dimensions and possible configurations in interaction with a surface.
- **Figure S4**: QCM-D frequency shifts fittings for adsorption of WGA solution at a concentration of 50 µg/mL on chitosan of different DAs (0.5%, 15%, 35%, 54%, 67%, 76%).

Declaration of competing interest: The authors declare no competing financial interest.

Data availability statement: The data supporting this article have been included as part of the ESI. All additional data reported in the paper will be shared by the corresponding author upon request.

Corresponding Author: Guillaume Sudre.

Funding Sources: This study was funded by the French National Research Agency (ANR) under the ArtiCute project (ANR-21-CE20-0001).

Acknowledgments: The authors thank Agnès Crépet (IMP, UCBL, CNRS Villeurbanne) and the Chromatography Plateform at Institut de Chimie de Lyon for the SEC analyses.

Abbreviations: AcOH, acetic acid; SEC, size exclusion spectroscopy; NMR, nuclear magnetic resonance; DA, degree of acetylation; GlcN, D-glucosamine; GlcNAc, *N*-acetyl-D-glucosamine; CBD, chitin-binding domain; WGA, wheat germ agglutinin; IGG, immunoglobulin G; QCM-D, quartz crystal microbalance with dissipation monitoring; SPR, surface plasmon resonance; PDB, protein data bank; LC, low concentration; HC, high concentration.

6. REFERENCES

[1] G.B. Eshun, H.A. Crapo, I. Yazgan, L. Cronmiller, O.A. Sadik, Sugar–Lectin Interactions for Direct and Selective Detection of Escherichia coli Bacteria Using QCM Biosensor, Biosensors 13 (2023) 337. https://doi.org/10.3390/bios13030337.

[2] P.H.L. Lima, S.V.A. Pereira, R.B. Rabello, E. Rodriguez-Castellón, M.M. Beppu, P. Chevallier, D. Mantovani, R.S. Vieira, Blood protein adsorption on sulfonated chitosan and κ-carrageenan films, Colloids Surf. B Biointerfaces 111 (2013) 719–725. https://doi.org/10.1016/j.colsurfb.2013.06.002.

[3] K. Shang, S. Song, Y. Cheng, L. Guo, Y. Pei, X. Lv, T. Aastrup, Z. Pei, Fabrication of Carbohydrate Chips Based on Polydopamine for Real-Time Determination of Carbohydrate–Lectin Interactions by QCM Biosensor, Polymers 10 (2018) 1275. https://doi.org/10.3390/polym10111275.

[4] H. Černocká, N. Izadi, V. Ostatná, S. Strmečki, BSA-Polysaccharide Interactions at Negatively Charged Electrode Surface. Effects of Current Density., Electroanalysis 31 (2019) 2007–2011. https://doi.org/10.1002/elan.201900231.

[5] Q. Gong, L. Chen, J. Wang, F. Yuan, Z. Ma, G. Chen, Y. Huang, Y. Miao, T. Liu, X.-X. Zhang, Q. Yang, J. Yu, Coassembly of a New Insect Cuticular Protein and Chitosan via Liquid–Liquid Phase Separation, Biomacromolecules 23 (2022) 2562–2571. https://doi.org/10.1021/acs.biomac.2c00261.

[6] K. De Schutter, E.J.M. Van Damme, Protein-Carbohydrate Interactions, and Beyond …, Molecules 20 (2015) 15202–15205. https://doi.org/10.3390/molecules200815202.

[7] M. Rinaudo, Chitin and chitosan: Properties and applications, Prog. Polym. Sci. 31 (2006) 603–632. https://doi.org/10.1016/j.progpolymsci.2006.06.001.

[8] J. Kumirska, M.X. Weinhold, S. Steudte, J. Thöming, K. Brzozowski, P. Stepnowski, Determination of the pattern of acetylation of chitosan samples: Comparison of evaluation methods and some validation parameters, Int. J. Biol. Macromol. 45 (2009) 56–60. https://doi.org/10.1016/j.ijbiomac.2009.04.002.

[9] J. Wattjes, S. Sreekumar, C. Richter, S. Cord-Landwehr, R. Singh, N.E. El Gueddari, B.M. Moerschbacher, Patterns matter part 1: Chitosan polymers with non-random patterns of acetylation, React. Funct. Polym. 151 (2020) 104583. https://doi.org/10.1016/j.reactfunctpolym.2020.104583.

[10] K.M. Vårum, M.W. Anthonsen, H. Grasdalen, O. Smidsrød, K.M. Vårum, M.W. Anthonsen, H. Grasdalen, O. Smidsrød, 13C-n.m.r. studies of the acetylation sequences in partially N-

deacetylated chitins (chitosans), Carbohydr. Res. 217 (1991) 19–27. https://doi.org/10.1016/0008-6215(91)84113-s.
[11] K.M. Vårum, M.W. Anthonsen, H. Grasdalen, O. Smidsrød, Determination of the degree of N-acetylation and the distribution of N-acetyl groups in partially N-deacetylated chitins (chitosans) by high-field n.m.r. spectroscopy, Carbohydr. Res. 211 (1991) 17–23. https://doi.org/10.1016/0008-6215(91)84142-2.
[12] J. Jiménez-Barbero, F. Javier Cañada, J.L. Asensio, N. Aboitiz, P. Vidal, A. Canales, P. Groves, H.-J. Gabius, H.-C. Siebert, Hevein Domains: An Attractive Model to Study Carbohydrate–Protein Interactions at Atomic Resolution, in: Adv. Carbohydr. Chem. Biochem., Elsevier, 2006: pp. 303–354. https://doi.org/10.1016/S0065-2318(06)60007-3.
[13] W.J. Peumans, E.J. Van Damme, Lectins as plant defense proteins., Plant Physiol. 109 (1995) 347–352. https://doi.org/10.1104/pp.109.2.347.
[14] J.L. Asensio, F.J. Cañada, H.-C. Siebert, J. Laynez, A. Poveda, P.M. Nieto, U. Soedjanaamadja, H.-J. Gabius, J. Jiménez-Barbero, Structural basis for chitin recognition by defense proteins: GlcNAc residues are bound in a multivalent fashion by extended binding sites in hevein domains, Chem. Biol. 7 (2000) 529–543. https://doi.org/10.1016/S1074-5521(00)00136-8.
[15] J.L. Asensio, F.J. Canada, M. Bruix, A. Rodriguez-Romero, J. Jimenez-Barbero, The interaction of hevein with N-acetylglucosamine-containing oligosaccharides. Solution structure of hevein complexed to chitobiose, Eur. J. Biochem. 230 (1995) 621–633. https://doi.org/10.1111/j.1432-1033.1995.tb20604.x.
[16] J.L. Asensio, F.J. Cañada, M. Bruix, C. González, N. Khiar, A. Rodríguez-Romero, J. Jiménez-Barbero, NMR investigations of protein-carbohydrate interactions: refined three-dimensional structure of the complex between hevein and methyl beta-chitobioside, Glycobiology 8 (1998) 569–577. https://doi.org/10.1093/glycob/8.6.569.
[17] J.C. Martins, D. Maes, R. Loris, H.A. Pepermans, L. Wyns, R. Willem, P. Verheyden, H NMR study of the solution structure of Ac-AMP2, a sugar binding antimicrobial protein isolated from Amaranthus caudatus, J. Mol. Biol. 258 (1996) 322–333. https://doi.org/10.1006/jmbi.1996.0253.
[18] H.-C. Siebert, R. Kaptein, J.J. Beintema, U.M. Soedjanaatmadja, C.S. Wright, A. Rice, R.G. Kleineidam, S. Kruse, R. Schauer, P.J.W. Pouwels, J.P. Kamerling, H.-J. Gabius, J.F.G. Vliegenthart, Carbohydrate-protein interaction studies by laser photo CIDNP NMR methods, Glycoconj. J. 14 (1997) 531–534. https://doi.org/10.1023/a:1018572023153.
[19] K. el Biari, Á. Gaudioso, M.C. Fernández-Alonso, J. Jiménez-Barbero, F.J. Cañada, Peptidoglycan Recognition by Wheat Germ Agglutinin. A View by NMR, Nat. Prod. Commun. 14 (2019) 1934578X1984924. https://doi.org/10.1177/1934578X19849240.
[20] J.F. Espinosa, J.L. Asensio, J.L. García, J. Laynez, M. Bruix, C. Wright, H.-C. Siebert, H.-J. Gabius, F.J. Cañada, J. Jiménez-Barbero, NMR investigations of protein-carbohydrate interactions: Binding studies and refined three-dimensional solution structure of the complex between the B domain of wheat germ agglutinin and N,N′,N″-triacetylchi, Eur. J. Biochem. 267 (2000) 3965–3978. https://doi.org/10.1046/j.1432-1327.2000.01415.x.
[21] C.S. Wright, Structural comparison of the two distinct sugar binding sites in wheat germ agglutinin isolectin II, J. Mol. Biol. 178 (1984) 91–104. https://doi.org/10.1016/0022-2836(84)90232-8.
[22] C.S. Wright, 2·2 Å resolution structure analysis of two refined N-acetylneuraminyl-lactose—Wheat germ agglutinin isolectin complexes, J. Mol. Biol. 215 (1990) 635–651. https://doi.org/10.1016/S0022-2836(05)80174-3.
[23] C.S. Wright, Crystal structure of a wheat germ agglutinin/glycophorin-sialoglycopeptide receptor complex. Structural basis for cooperative lectin-cell binding., J. Biol. Chem. 267 (1992) 14345–14352. https://doi.org/10.1016/S0021-9258(19)49718-4.
[24] H.C. Siebert, C.W. von der Lieth, R. Kaptein, J.J. Beintema, K. Dijkstra, N. van Nuland, U.M. Soedjanaatmadja, A. Rice, J.F. Vliegenthart, C.S. Wright, H.J. Gabius, Role of aromatic amino acids in carbohydrate binding of plant lectins: laser photo chemically induced dynamic nuclear polarization study of hevein domain-containing lectins, Proteins 28 (1997) 268–284. https://doi.org/10.1007/s0089460020351.

[25] K. Matsuoka, Biological Evaluation of Multivalent-Type N-Acetyl-D-Glucosamine (GlcNAc) Conjugates for Wheat Germ Agglutinin (WGA) by the Surface Plasmon Resonance (SPR) Method, SOJ Biochem. 2 (2016) 1–7. https://doi.org/10.15226/2376-4589/2/3/00118.
[26] M. Reynolds, M. Marradi, A. Imberty, S. Penadés, S. Pérez, Multivalent gold glycoclusters: high affinity molecular recognition by bacterial lectin PA-IL, Chem. Weinh. Bergstr. Ger. 18 (2012) 4264–4273. https://doi.org/10.1002/chem.201102034.
[27] S. Vogt, M. Kelkenberg, T. Nöll, B. Steinhoff, H. Schönherr, H. Merzendorfer, G. Nöll, Rapid determination of binding parameters of chitin binding domains using chitin-coated quartz crystal microbalance sensor chips, The Analyst 143 (2018) 5255–5263. https://doi.org/10.1039/C8AN01453A.
[28] T. Wangchareansak, C. Sangma, P. Ngernmeesri, A. Thitithanyanont, P.A. Lieberzeit, Self-assembled glucosamine monolayers as biomimetic receptors for detecting WGA lectin and influenza virus with a quartz crystal microbalance, Anal. Bioanal. Chem. 405 (2013) 6471–6478. https://doi.org/10.1007/s00216-013-7057-0.
[29] Z. Pei, H. Anderson, T. Aastrup, O. Ramström, Study of real-time lectin-carbohydrate interactions on the surface of a quartz crystal microbalance, Biosens. Bioelectron. 21 (2005) 60–66. https://doi.org/10.1016/j.bios.2004.10.006.
[30] M.-C. Radulescu, B. Bucur, M.P. Bucur, G.L. Radu, Quality control method based on quartz crystal microbalance and WGA for flour milled from germinated wheat, Eur. Food Res. Technol. 229 (2009) 833–840. https://doi.org/10.1007/s00217-009-1120-2.
[31] M.M. Pedroso, A.M. Watanabe, M.C. Roque-Barreira, P.R. Bueno, R.C. Faria, Quartz Crystal Microbalance monitoring the real-time binding of lectin with carbohydrate with high and low molecular mass, Microchem. J. 89 (2008) 153–158. https://doi.org/10.1016/j.microc.2008.02.001.
[32] C. Schatz, C. Viton, T. Delair, C. Pichot, A. Domard, Typical physicochemical behaviors of chitosan in aqueous solution, Biomacromolecules 4 (2003) 641–648. https://doi.org/10.1021/bm025724c.
[33] L. Vachoud, N. Zydowicz, A. Domard, Formation and characterisation of a physical chitin gel, Carbohydr. Res. 302 (1997) 169–177. https://doi.org/10.1016/S0008-6215(97)00126-2.
[34] A. Hirai, H. Odani, A. Nakajima, Determination of degree of deacetylation of chitosan by 1H NMR spectroscopy, Polym. Bull. 26 (1991) 87–94. https://doi.org/10.1007/BF00299352.
[35] A. Moussa, A. Crépet, C. Ladavière, S. Trombotto, Reducing-end “clickable” functionalizations of chitosan oligomers for the synthesis of chitosan-based diblock copolymers, Carbohydr. Polym. 219 (2019) 387–394. https://doi.org/10.1016/j.carbpol.2019.04.078.
[36] L. Basso, G. Sudre, D. Albertini, Y. Rahbé, L. David, Chitosan surface interaction platform for protein binding quantification by fluorescence microscopy, application to the specificity of CBD proteins, Carbohydr. Polym. (2025) 123321. https://doi.org/10.1016/j.carbpol.2025.123321.
[37] D. Yang, R. Kroe-Barrett, S. Singh, T. Laue, IgG Charge: Practical and Biological Implications, Antibodies 8 (2019) 24. https://doi.org/10.3390/antib8010024.
[38] M. Monsigny, C. Sene, A. Obrenovitch, A.-C. Roche, F. Delmotte, E. Boschetti, Properties of Succinylated Wheat-Germ Agglutinin, Eur. J. Biochem. 98 (1979) 39–45. https://doi.org/10.1111/j.1432-1033.1979.tb13157.x.
[39] K. Sugawara, A. Terauchi, N. Kamiya, G. Hirabayashi, H. Kuramitz, Voltammetric Behaviors of Wheat-Germ Agglutinin on a Chitin-modified Carbon-Paste Electrode, Anal. Sci. 24 (2008) 583–587. https://doi.org/10.2116/analsci.24.583.
[40] B. Jachimska, S. Świątek, J.I. Loch, K. Lewiński, T. Luxbacher, Adsorption effectiveness of β-lactoglobulin onto gold surface determined by quartz crystal microbalance, Bioelectrochemistry 121 (2018) 95–104. https://doi.org/10.1016/j.bioelechem.2018.01.010.
[41] C. Garreau, L. Chiappisi, S. Micciulla, N. Blanc, I. Morfin, A. Desorme, T. Mignot, S. Trombotto, T. Delair, G. Sudre, Grafted chitosan thin films of various degrees of acetylation as a reusable platform for the investigation of biological interactions, Int. J. Biol. Macromol. (2023) 125565. https://doi.org/10.1016/j.ijbiomac.2023.125565.
[42] J. Becerra, G. Sudre, I. Royaud, R. Montserret, B. Verrier, C. Rochas, T. Delair, L. David, Tuning the Hydrophilic/Hydrophobic Balance to Control the Structure of Chitosan Films and

Their Protein Release Behavior, AAPS PharmSciTech 18 (2017) 1070–1083. https://doi.org/10.1208/s12249-016-0678-9.
[43] A. Dolatshahi-Pirouz, T. Jensen, M. Foss, J. Chevallier, F. Besenbacher, Enhanced Surface Activation of Fibronectin upon Adsorption on Hydroxyapatite, Langmuir 25 (2009) 2971–2978. https://doi.org/10.1021/la803142u.
[44] M.B. Hovgaard, K. Rechendorff, J. Chevallier, M. Foss, F. Besenbacher, Fibronectin Adsorption on Tantalum: The Influence of Nanoroughness, J. Phys. Chem. B 112 (2008) 8241–8249. https://doi.org/10.1021/jp801103n.
[45] P.J. Molino, M.J. Higgins, P.C. Innis, Robert.M.I. Kapsa, G.G. Wallace, Fibronectin and Bovine Serum Albumin Adsorption and Conformational Dynamics on Inherently Conducting Polymers: A QCM-D Study, Langmuir 28 (2012) 8433–8445. https://doi.org/10.1021/la300692y.
[46] P. Hampitak, D. Melendrez, M. Iliut, M. Fresquet, N. Parsons, B. Spencer, T.A. Jowitt, A. Vijayaraghavan, Protein interactions and conformations on graphene-based materials mapped using a quartz-crystal microbalance with dissipation monitoring (QCM-D), Carbon 165 (2020) 317–327. https://doi.org/10.1016/j.carbon.2020.04.093.
[47] P. Komorek, E. Martin, B. Jachimska, Adsorption and Conformation Behavior of Lysozyme on a Gold Surface Determined by QCM-D, MP-SPR, and FTIR, Int. J. Mol. Sci. 22 (2021) 1322. https://doi.org/10.3390/ijms22031322.
[48] Y. Zhang, X. Wang, P. Wang, J. Song, Y. Jin, O.J. Rojas, Interactions between type A carbohydrate binding modules and cellulose studied with a quartz crystal microbalance with dissipation monitoring, Cellulose 27 (2020) 3661–3675. https://doi.org/10.1007/s10570-020-03070-4.
[49] M. del C. Portillo-Téllez, M. Bello, G. Salcedo, G. Gutiérrez, V. Gómez-Vidales, E. García-Hernández, Folding and Homodimerization of Wheat Germ Agglutinin, Biophys. J. 101 (2011) 1423–1431. https://doi.org/10.1016/j.bpj.2011.07.037.
[50] M. Gagliardi, L. Colagiorgio, M. Cecchini, A Fast and Reliable Method Based on QCM-D Instrumentation for the Screening of Nanoparticle/Blood Protein Interactions, Biosensors 13 (2023) 607. https://doi.org/10.3390/bios13060607.

Supporting information for:

Chitin-binding protein behavior at chitosan interface studied by quartz crystal microbalance with dissipation monitoring (QCM-D): binding quantification, orientation and affinity constants

Lisa Basso [a], Clémence Vuillet [a], Yvan Rahbé [b], Laurent David [a], Aurélia Charlot [a], Guillaume Sudre [a]

[a] *Universite Claude Bernard Lyon 1, INSA Lyon, Université Jean Monnet, CNRS UMR 5223, Ingénierie des Matériaux Polymères (IMP) F-69622 Villeurbanne Cédex, France.*

[b] *Universite Claude Bernard Lyon 1, INSA Lyon, INRAE, CNRS UMR 5240, Microbiologie, Adaptation et Pathogénie (MAP), F-69621 Villeurbanne, France*

Materials

Chitosan from shrimp shells was purchased from Mahtani Chitosan Ltd (Veraval, India, batch type 244 LG). The degree of acetylation (DA) was determined by ^{1}H NMR thanks to the method of Hirai *et al*. [1] and was found equal to 0.5%. Chitosan mass average molar mass was determined by size exclusion chromatography coupled with Multiangle Laser Light Scattering (M_w = 190 kg/mol, dispersity $Đ$ = 2.3). Acetic acid (AcOH, > 99% w/w), ammonium hydroxide (NH_4OH, 28% w/w), deuterium oxide (99.9% D), HEPES buffer (powder form), lectin from *Triticum Vulgaris* (WGA, lyophilized, immunoglobulin-G (IGG) from human serum were purchased from Sigma Aldrich. Acetic anhydride (> 99% w/w) was purchased from Carlo Erba. Gold-coated quartz crystal sensors QSX301 were purchased from Biolin Scientific (Gothenburg, Sweden). Ultrapure Milli-Q water was obtained thanks to an ultrapure water system (Milli-Q Simplicity® water purification system, with resistivity of 18.2 MΩ.cm).

Data analysis

The Sauerbrey equation was used to convert the resonance frequency shift to the adsorbed mass of analyte per unit area. The thickness of the deposited layer of analyte (at the swollen state) can be estimated from the data thanks to the layer density (typical densities were provided in the software and were evaluated at 1050 g/L for hydrated polysaccharides and 1100 g/L for hydrated proteins). The frequency change was fitted to either an exponential or a biexponential function and modelling parameters were used to determine the affinity constants k_{obs}.

$$R + L \underset{k_{off}}{\overset{k_{on}}{\rightleftharpoons}} RL$$

$$y = A + B_1 \times e^{-t/\tau_1} \quad (2)$$

$$\frac{1}{\tau_1} = k_{obs} = k_{on} \times C + k_{off}$$

$$R + L \underset{k_{off,1}}{\overset{k_{on,1}}{\rightleftharpoons}} RL \underset{k_{off,2}}{\overset{k_{on,2}}{\rightleftharpoons}} RL^*$$

$$y = A + B_1 \times e^{-t/\tau_1} + B_2 \times e^{-t/\tau_2} \quad (3)$$

$$\frac{1}{\tau_1} = k_{obs,1} = k_{on,1} \times C + k_{off,1} \qquad \frac{1}{\tau_2} = k_{obs,2} = k_{on,2} \times C + k_{off,2}$$

Where *R* is the receptor, *L* the ligand, k_{on} the association constant, k_{off} the dissociation constant and k_{obs} the observed association constant.

In enzyme kinetics, the exponential function (2) is typically used to model a one-step association. The bi-exponential function (3) is used to model a two-step association, in which the first step is the ligand to receptor binding and the second step is the change in conformation of one or both of the associated parts.[2,3] In the context of this study, RL and RL* may represent two different surface configurations of the protein interacting with chitosans films. Such modellings allow to identify or confirm the interaction model and determine the observed association rate constants (k_{obs}) of ligand-receptor binding.[4]

WGA and IGG adsorption on bare gold

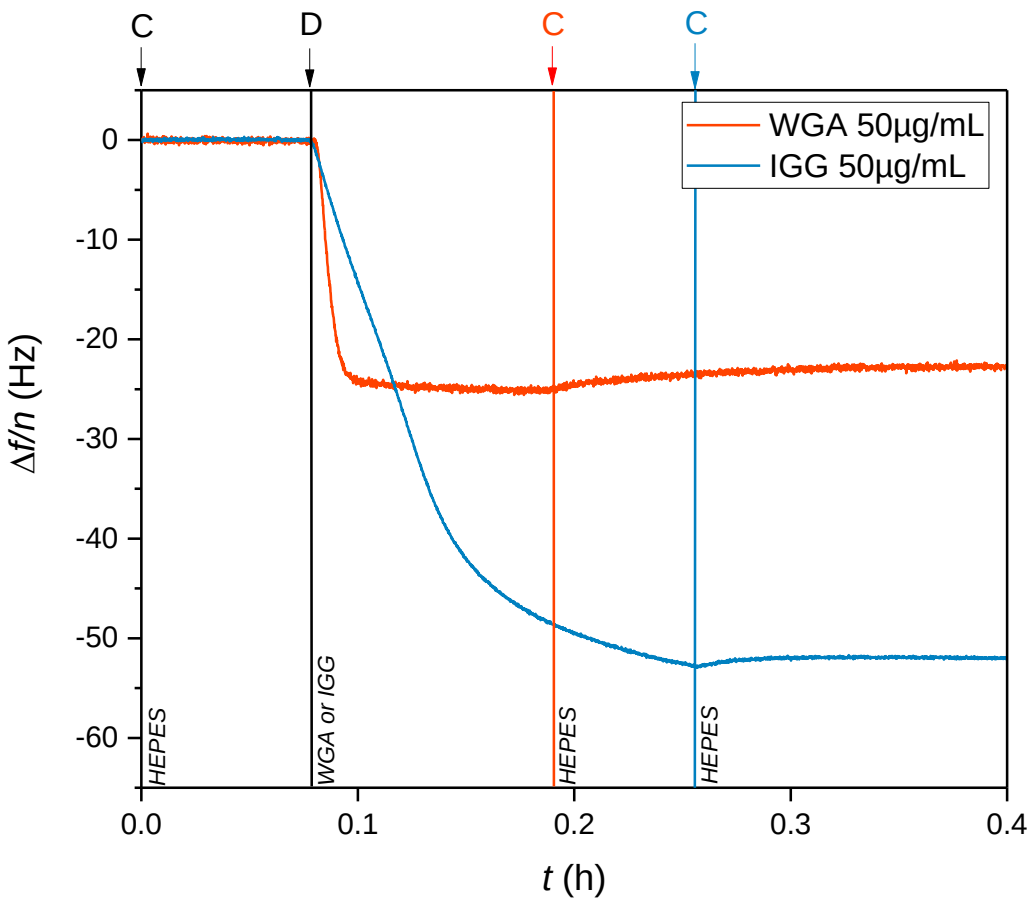

Figure S1: *QCM-D frequency shifts result for adsorption of WGA and IGG on bare gold sensors at pH 7. Δf/n corresponds to the shift in frequency of the n^{th} overtone. The letters C and D correspond to the solutions used for QCM-D experiments (C: HEPES 0.01M pH7; D: Protein (WGA or IGG) 50µg/mL in buffer C. The changes in solution flows are marked by an arrow and a vertical line.*

WGA adsorption on chitosan DA0.5% at 2 different concentrations

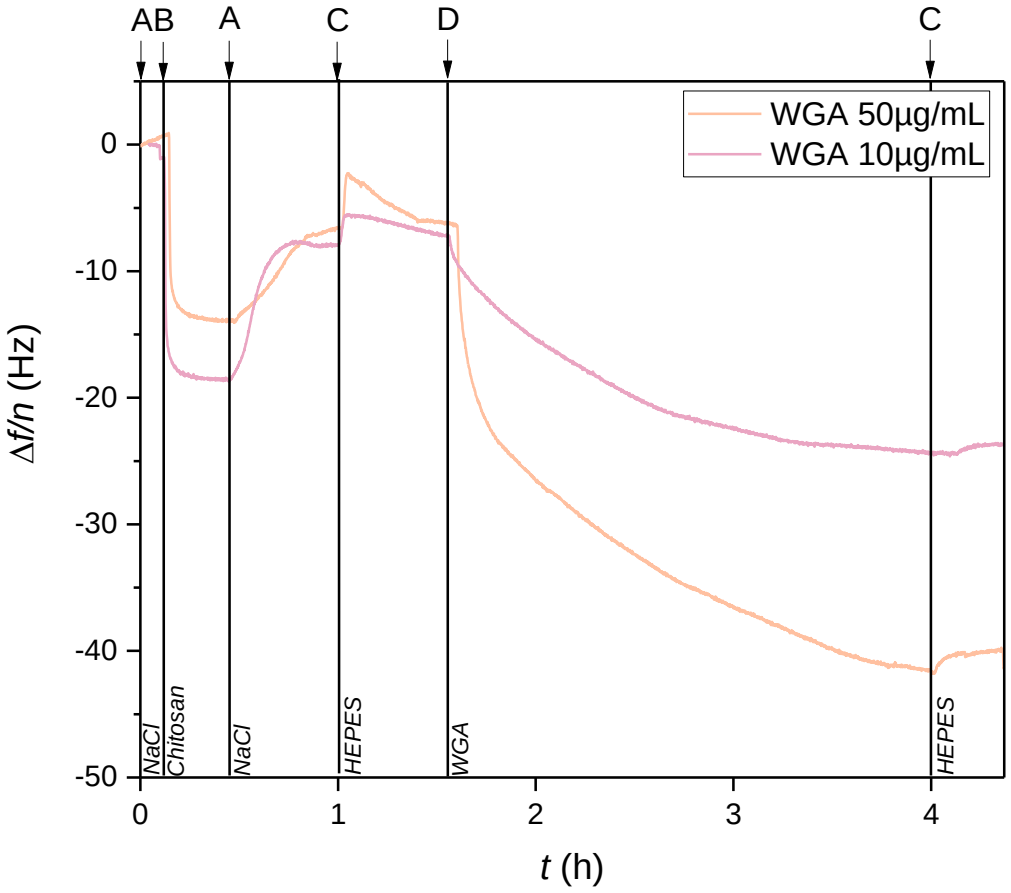

Figure S2: *QCM-D frequency shifts result for adsorption of WGA of concentration 50 µg/mL (orange) or 10 µg/mL (blue) on chitosan of DA 0.5% at pH 7.0. The letters A, B, C and D correspond to the solutions used for QCM-D experiments (A: [NaCl] = 0.15 M at pH 5.5; B: Chitosan of DA 0.5% at 0.5 mg/mL in buffer A; C: HEPES at 0.01 M at pH 7.0; D: WGA at 10 or 50 µg/mL in buffer C). The change in solution flows are marked by an arrow and a vertical line.*

WGA dimer protein dimensions and possible configurations in interaction with a surface

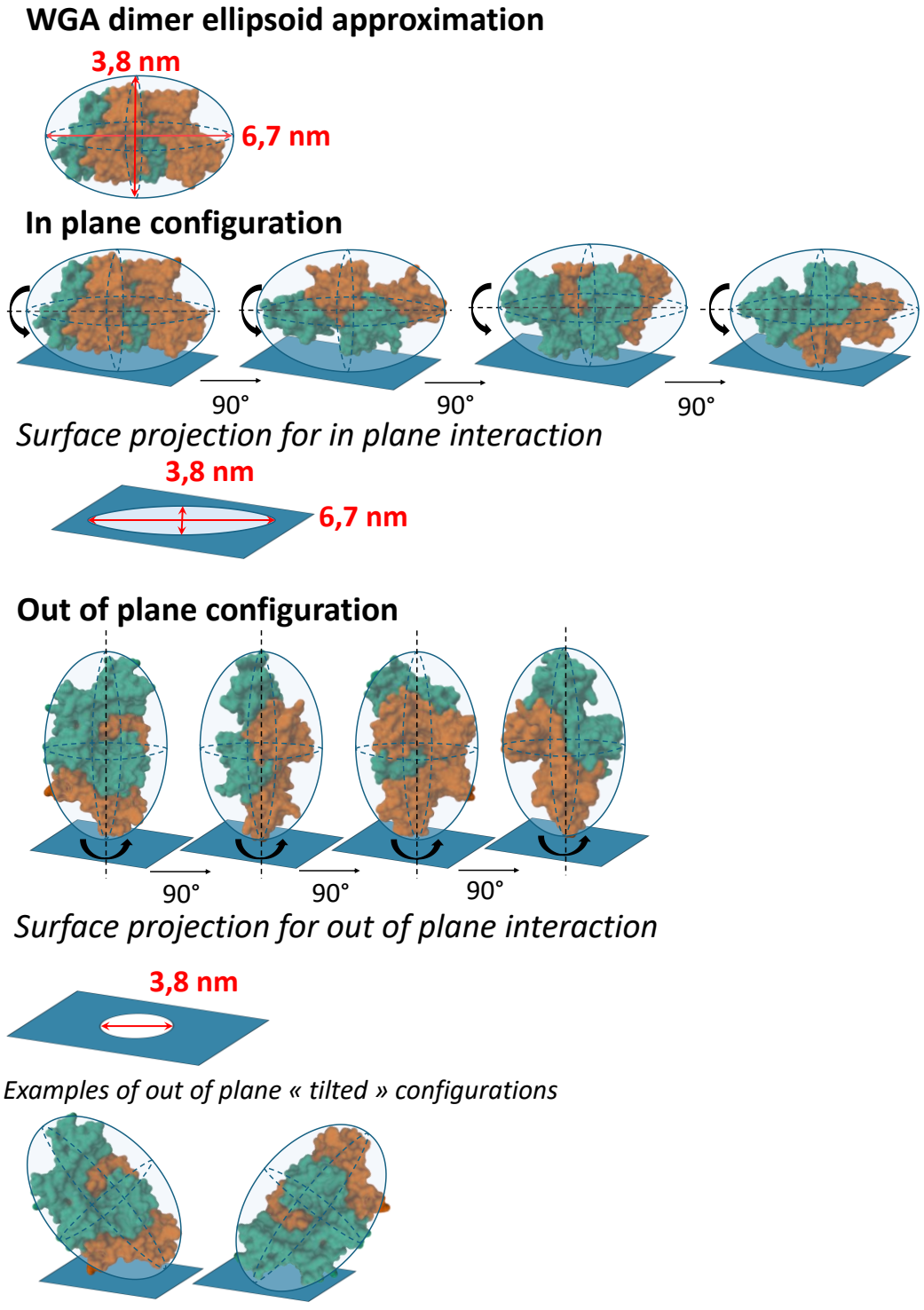

Figure S3: *Dimensions of WGA dimer protein (Uniprot®: P10968) as measured on the crystal 3D structure of PDB: 2UVO and ellipsoid approximation. In plane and out of plane configurations of WGA when in interaction with a surface. The blue square represents the surface, monomer A is orange and monomer B is green.*

Kinetic modelling of WGA adsorption on chitosan layers of different DAs

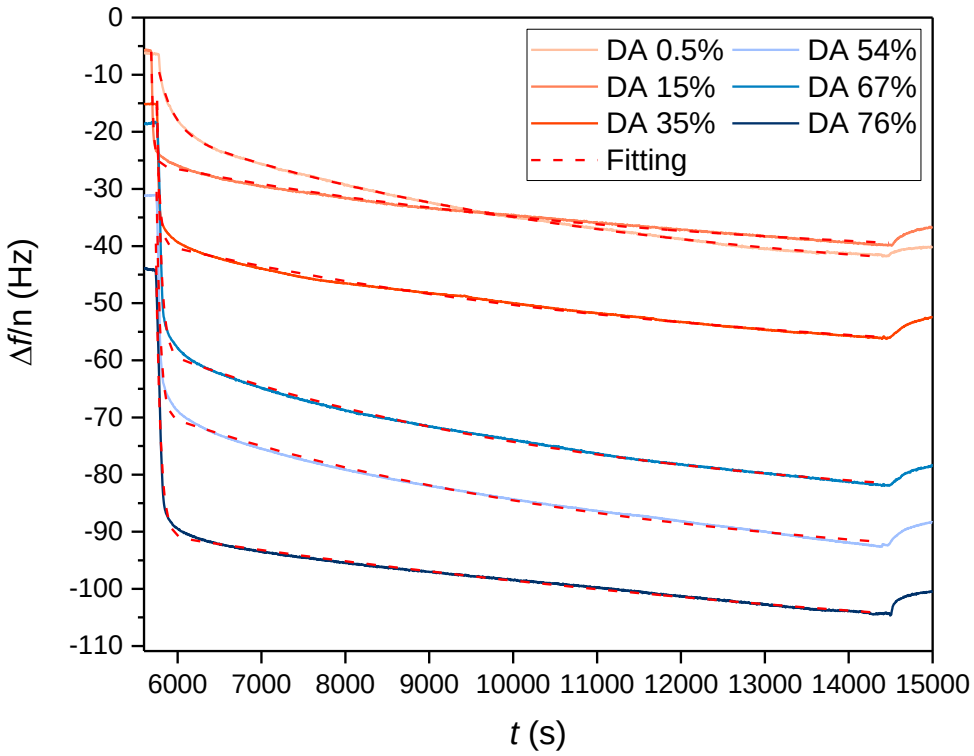

$$\frac{\Delta f}{n} = A + B_1 e^{-t/\tau_1} + B_2 e^{-t/\tau_2}$$

DA (%)	τ_1 (s)	τ_2 (s)	A (Hz)	B_1 (Hz)	B_2 (Hz)
0.5	183 ± 1	5415 ± 21	-47.47 ± 0.05	10.19 ± 0.04	27.36 ± 0.03
15	26.0 ± 0.5	5920 ± 62	-43.47 ± 0.09	10.2 ± 0.1	17.84 ± 0.08
35	34.5 ± 0.5	6359 ± 64	-61.6 ± 0.1	21.6 ± 0.2	22.0 ± 0.1
54	43.9 ± 0.4	5593 ± 47	-97.9 ± 0.1	34.5 ± 0.2	28.6 ± 0.1
67	49.6 ± 0.4	5177 ± 41	-86.8 ± 0.1	31.3 ± 0.1	28.32 ± 0.09
76	53.1 ± 0.4	11296 ± 288	-116.2 ± 0.5	47.7 ± 0.2	25.6 ± 0.4

Figure S4: *QCM-D frequency shifts bi-exponential fittings for adsorption of WGA solution of concentration 50µg/mL on chitosan layer of different DAs (0.5%, 15%, 35%, 54%, 67%, 76%) at pH 7.0.*

References

[1] A. Hirai, H. Odani, A. Nakajima, Determination of degree of deacetylation of chitosan by 1H NMR spectroscopy, Polymer Bulletin 26 (1991) 87–94. https://doi.org/10.1007/BF00299352.

[2] T.D. Pollard, E.M. De La Cruz, Take advantage of time in your experiments: a guide to simple, informative kinetics assays, MBoC 24 (2013) 1103–1110. https://doi.org/10.1091/mbc.e13-01-0030.

[3] S.R.J. Hoare, Analyzing Kinetic Binding Data, in: S. Markossian, A. Grossman, K. Brimacombe, M. Arkin, D. Auld, C. Austin, J. Baell, T.D.Y. Chung, N.P. Coussens, J.L. Dahlin, V. Devanarayan, T.L. Foley, M. Glicksman, K. Gorshkov, J.V. Haas, M.D. Hall, S. Hoare, J. Inglese, P.W. Iversen, S.C. Kales, M. Lal-Nag, Z. Li, J. McGee, O. McManus, T. Riss, P. Saradjian, G.S. Sittampalam, M. Tarselli, O.J. Trask, Y. Wang, J.R. Weidner, M.J. Wildey, K. Wilson, M. Xia, X. Xu (Eds.), Assay Guidance Manual, Eli Lilly & Company and the National Center for Advancing Translational Sciences, Bethesda (MD), 2004. http://www.ncbi.nlm.nih.gov/books/NBK569501/ (accessed February 29, 2024).

[4] P. Komorek, E. Martin, B. Jachimska, Adsorption and Conformation Behavior of Lysozyme on a Gold Surface Determined by QCM-D, MP-SPR, and FTIR, International Journal of Molecular Sciences 22 (2021) 1322. https://doi.org/10.3390/ijms22031322.